Skyrmion lattice and intrinsic angular momentum effect in the *A* phase of superfluid ^{3}He under rotation

Masanori Ichioka, Takeshi Mizushima, and Kazushige Machida
Department of Physics, Okayama University, Okayama 700-8530, Japan
(Received 18 August 2010; published 23 September 2010)

As an example of the skyrmion lattice, the structure of Mermin-Ho vortex lattice in superfluids ^{3}He is studied by self-consistent Eilenberger theory and by Bogoliubov-de Gennes theory. We identify how the intrinsic orbital angular momentum **l** of *p*-wave Cooper pairs contributes to spatial structures of the pair potential, current flow, and quasiparticle states. There are two types of vortices depending on the **l** direction relative to rotation. Only one of them has zero-energy bound states appearing even in coreless vortices due to intrinsic topological reasons.

DOI: 10.1103/PhysRevB.82.094516 PACS number(s): 67.30.he, 74.20.Rp, 74.25.Uv

I. INTRODUCTION

Skyrmion is one of the emergent topological objects, exemplified by monopole, meron, or hedgehog, encompassing a wide range of research fields from particle physics[1] to condensed-matter physics.[2–4] The low-lying Fermionic excitations associated with the localized topological objects play a major role in governing the physical behaviors which reflect those topological nature. In the condensed-matter context skyrmion usually forms a periodic lattice, as shown in Fig. 1(a), to be detected by a macroscopic observation. Except for a few example such as recent clear observation of remarkable skyrmion lattice in a weak itinerant ferromagnet of MnSi and $Fe_{1-x}Co_xSi$ under a magnetic field,[5,6] there is not much concrete system accessible experimentally.

Superfluid ^{3}He,[7,8] which is a typical multicomponent order-parameter system with *p*-wave pairing, provides us a fertile research field to investigate the interplay between the topology and the low-lying Fermionic excitations of quasiparticles, and gains recently renewed interest because of possible existence of Majorana quasiparticle[9–13] with a zero-energy Fermionic excitation. Here we focus on the *A* phase where the Cooper pairs have intrinsic angular momentum (IAM) denoted by *l* vector $\mathbf{l}=(l_x,l_y,l_z)$ whose direction is degenerate in a bulk. Note that the pairing component $p_+=p_x+ip_y$ ($p_-=p_x-ip_y$) gives positive (negative) l_z. IAM plays a fundamental role in describing the spatial structure of quasiparticles and thermodynamic behaviors in a system.[7,8]

As a concrete realization of the skyrmion lattice, we consider the Mermin-Ho (MH) vortex lattice and texture.[14] The MH vortices were observed in superfluid ^{3}He *A* phase experimentally under rotation,[15,16] and the stability of MH vortex lattice was supported by theoretical studies using Ginzburg-Landau theory.[17,18] In Refs. 15 and 18, LV1 (locked vortex 1) corresponds to the MH vortex lattice. The MH vortex is a building block embedded in the MH texture, forming a periodic array. It has a soft core in contrast with conventional singular hard core vortex in scalar order-parameter phases. Since the *l*-vector direction can be spherically rotatable depending on positions, outside the MH vortex core *l* vector could be directed to (x,y) plane. The coreless vortex structure can be formed merely by rotating the *l*-vector direction by 360° around the vortex, keeping the total order-parameter amplitude constant. At the core of the MH vortex, *l* vector can be directed to $+z$ or $-z$ direction.

The soft core MH vortex is an interesting topological object because the background *A* phase is maintained throughout the whole system without any singular point. Yet MH vortex is stable under rotation. The low-lying Fermionic excitations associated with this remarkable MH texture are intriguing because they reflect faithfully and directly the underlying topological structure of skyrmion lattice. Therefore we can analyze the intimate interplay between the low-lying excitations and topology. We uncover a generic question of

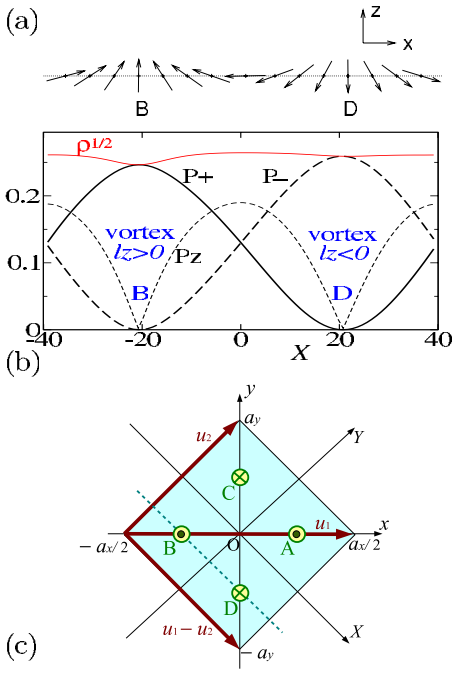

FIG. 1. (Color online) (a) Skyrmion structure of *l* vectors around $MH_\uparrow$ at B and $MH_\downarrow$ at D. (b) Profiles of pair potentials; $|\eta_+(\mathbf{r})|$ for p_+ component, $|\eta_-(\mathbf{r})|$ for p_- component, $|\eta_z(\mathbf{r})|$ for p_z component, and pair amplitude $\sqrt{\rho(\mathbf{r})}$, obtained by self-consistent Eilenberger theory. $\Omega=0.004\Omega_0$ and $T=0.9T_c$. (c) Unit cell of Mermin-Ho vortex lattice, including four vortices. $MH_\uparrow(MH_\downarrow)$ vortices with $l_z>0$ ($l_z<0$) are located at positions A and B (C and D). $\mathbf{u}_1-\mathbf{u}_2$ and $\mathbf{u}_2$ are unit vectors. Horizontal axis in (a) and (b) is along the dashed line in (c).

the presence or absence of the vortex bound state in multicomponent superfluids with a higher orbital pairing $p_\pm$, which could realize the time reversal symmetry-breaking pairing, and give rise to IAM. We study the interplay between the local IAM and vortex-winding number. This interplay yields nontrivial effects on the above question as we will see soon.

The vortex lattice structure formed by MH vortices is unconventional, where the unit cell of vortex lattice contains two positive l_z vortices ($MH_\uparrow$) and two negative l_z vortices ($MH_\downarrow$), as shown in Fig. 1(c).[7,17,18] In nomenclature in Ref. 8, $MH_\downarrow$ corresponds to MT (mixed-twist) vortex. It is shown below that these two kinds of the cores exhibit completely different low-energy excitation spectra. So far, most of the study for the MH vortex lattice was done by phenomenological Ginzburg-Landau theory.[17,18] According to our microscopic calculations based on Eilenberger theory[19–22] backed up by the full quantum mechanical Bogoliubov-de Gennes (BdG) theory, we succeeded in uncovering the nontrivial physical mechanism of the interplay between IAM and winding number. We note that MH vortex structures are also expected in spinor Bose-Einstein condensate in ultracold Bose gases under rotation.[3,4,23]

After Sec. I, we describe our formulation by self-consistent Eilenberger theory for MH vortex lattice in Sec. II. We study the spatial structure of order parameter and mass current in Sec. III, and low-energy quasiparticle states in Sec. IV, based on the Eilenberger theory. The quasiparticle structure is examined also by BdG calculations in Sec V. The last section is devoted to summary and discussions.

II. EILENBERGER THEORY FOR MERMIN-HO VORTEX LATTICE

The quasiclassical Eilenberger theory is quantitatively valid when $\xi \gg 1/k_F$ (k_F is the Fermi wave number and ξ is the superfluid coherence length), and has been used in the study of ^{3}He superfluidity.[24–27] In the clean limit, the quasiclassical Green's functions $g(\omega_n,\mathbf{k},\mathbf{r})$, $f(\omega_n,\mathbf{k},\mathbf{r})$, and $f^\dagger(\omega_n,\mathbf{k},\mathbf{r})$ are calculated by the Eilenberger equation,[19–21]

$$\{\omega_n + \hat{\mathbf{v}}\cdot(\nabla + i\mathbf{A})\}f = \Delta g,$$

$$\{\omega_n - \hat{\mathbf{v}}\cdot(\nabla - i\mathbf{A})\}f^\dagger = \Delta^* g, \tag{1}$$

using the Riccati method,[22] where $g=(1-ff^\dagger)^{1/2}$, Re $g>0$, and $\hat{\mathbf{v}}=\mathbf{v}/v_{F0}$.

We consider all three orbital components of the p-wave pairing for the pair potential, as

$$\Delta(\mathbf{r},\mathbf{k}) = \eta_+(\mathbf{r})\varphi_+(\mathbf{k}) + \eta_-(\mathbf{r})\varphi_-(\mathbf{k}) + \eta_z(\mathbf{r})\varphi_z(\mathbf{k}), \tag{2}$$

$$\varphi_\pm(\mathbf{k}) = \mp\sqrt{\frac{3}{2}}\frac{k_x \pm ik_y}{k_F} = \mp\sqrt{\frac{3}{2}}\sin\theta_k e^{\pm i\phi_k}, \tag{3}$$

$$\varphi_z(\mathbf{k}) = \sqrt{3}\frac{k_z}{k_F} = \sqrt{3}\cos\theta_k, \tag{4}$$

where $\mathbf{k}=(k_x,k_y,k_z)=k_F(\sin\theta_k\cos\phi_k,\sin\theta_k\sin\phi_k,\cos\theta_k)$ is the relative momentum of the Cooper pair on the spherical Fermi surface, and $\mathbf{r}$ is the center-of-mass coordinate of the pair. The l vector is given by $l_x=\sqrt{2}\,\mathrm{Re}\{(\eta_+ + \eta_-)^*\eta_z\}/\rho$, $l_y=\sqrt{2}\,\mathrm{Im}\{(\eta_+ - \eta_-)^*\eta_z\}/\rho$, and $l_z=(|\eta_+|^2-|\eta_-|^2)/\rho$ with pair amplitude $\rho(\mathbf{r})=|\eta_+(\mathbf{r})|^2+|\eta_-(\mathbf{r})|^2+|\eta_z(\mathbf{r})|^2$.[23] For simplicity, we do not consider the spin components of the pair potential denoted as d vector since we neglect small dipole coupling of l vector and d vector. Therefore, the dipole length is infinity in our calculation. Since the Fermi surface is spherical in ^{3}He, the Fermi velocity is given by $\mathbf{v}=v_{F0}\mathbf{k}/k_F$. When the rotational axis is the z direction and angular velocity of rotation is Ω, $\mathbf{A}(\mathbf{r})=-\frac{1}{2}(0,0,\Omega)\times\mathbf{r}$. Throughout this paper, length, temperature, and Ω are scaled by R_0, superfluid transition temperature T_c, and Ω_0, respectively. Here, $R_0=\hbar v_{F0}/2\pi k_B T_c$, $\Omega_0=\phi_0/2\pi R_0^2$ with circulation quantum $\phi_0=h/2m$.[19] Matsubara frequency $\omega_n=(2n+1)\pi T$, energy E, and pair potential Δ are in a unit $\pi k_B T_c$. The order parameter η_j ($j=+,-,z$) is self-consistently calculated by

$$\eta_j(\mathbf{r}) = g_0 N_0 T \sum_{0<\omega_n<\omega_{cut}} \langle \varphi_j^*(\mathbf{k})(f + f^{\dagger *})\rangle_{\mathbf{k}} \tag{5}$$

with $(g_0N_0)^{-1}=\ln T + 2T\Sigma_{0<\omega_n<\omega_{cut}}|\omega_n|^{-1}$. $\langle\cdots\rangle_{\mathbf{k}}$ indicates the Fermi surface average, and N_0 is the density of states (DOS) at the Fermi energy in the normal state. We set energy cutoff of the pairing interaction as $\omega_{cut}=40k_BT_c$.

In the MH vortex lattice, a unit cell including four vortices is square,[17,18] as shown in Fig. 1(c) where two $MH_\uparrow$ are located at A and B and two $MH_\downarrow$ at C and D. Thus, we set a unit cell as $\mathbf{r}=W_1(\mathbf{u}_1-\mathbf{u}_2)+W_2\mathbf{u}_2$ ($|W_i|<0.5$, $i=1,2$) with unit vectors $\mathbf{u}_1=(a_x,0)$, $\mathbf{u}_2=(\frac{1}{2}a_x,a_y)$, and $a_y=\frac{1}{2}a_x$, where $a_xa_y\Omega=4\phi_0$. To consider the periodic boundary condition and the initial value for the pair potential, we introduce Abrikosov solution which has a single vortex within a unit cell, given as

$$\Psi(\mathbf{r}) = e^{i\pi xy/a_xa_y}\left(\frac{2a_y}{a_x}\right)^{1/4} \times \sum_{p=-\infty}^{\infty} e^{-\pi[(y+y_0)/a_y+p]^2a_y/a_x+2\pi i[p(x_0/a_x+\zeta p/2)+(y_0/a_y+p)x/a_x]} \tag{6}$$

when the vortex center is located at $(x_0,y_0)-\frac{1}{2}(\mathbf{u}_1+\mathbf{u}_2)$. This has translational relation

$$\Psi(\mathbf{r}+\mathbf{R}) = \Psi(\mathbf{r})e^{i\chi(\mathbf{r},\mathbf{R})}, \tag{7}$$

$$\chi(\mathbf{r},\mathbf{R}) = 2\pi\left\{\frac{1}{2}\left[(m+n\zeta)\frac{y}{a_y} - n\frac{x}{a_x}\right] + \frac{mn}{2} + (m+n\zeta)\frac{y_0}{a_y} - n\frac{x_0}{a_x}\right\} \tag{8}$$

for $\mathbf{R}=m\mathbf{u}_1+n\mathbf{u}_2$ (m,n: integer). We set $\chi_0(\mathbf{r},\mathbf{R})\equiv\chi(\mathbf{r},\mathbf{R})$ when the vortex center is located at (0,0). We prepare four Abrikosov solutions with different positions of the vortex centers. Abrikosov solution with the vortex center at $(\frac{1}{4}a_x,0)$, $(-\frac{1}{4}a_x,0)$, $(0,\frac{1}{2}a_y)$, and $(0,-\frac{1}{2}a_y)$ are, respectively, denoted as $\Psi_A(\mathbf{r})$, $\Psi_B(\mathbf{r})$, $\Psi_C(\mathbf{r})$, and $\Psi_D(\mathbf{r})$. In the MH vortex lattice,[17] $MH_\uparrow$ vortices with $l_z>0$ at A and B in Fig. 1(c) have the

phase winding $(w_+,w_z,w_-)=(0,1,2)$ around each vortex center, where w_+,w_z,w_- are, respectively, phase windings of the components η_+,η_z,η_- around a vortex center. Other vortices $\mathrm{MH}_\downarrow$ with $l_z<0$ at C and D have the phase winding $(w_+,w_z,w_-)=(2,1,0)$ around each vortex center. Therefore, as the initial states for MH vortex lattice,[17] we use

$$\eta_+(\mathbf{r}) = \{\Psi_C(\mathbf{r})\Psi_D(\mathbf{r})\}^2,$$

$$\eta_-(\mathbf{r}) = \{\Psi_A(\mathbf{r})\Psi_B(\mathbf{r})\}^2,$$

$$\eta_z(\mathbf{r}) = \Psi_A(\mathbf{r})\Psi_B(\mathbf{r})\Psi_C(\mathbf{r})\Psi_D(\mathbf{r}). \quad (9)$$

These states have the same translational relation

$$\eta_j(\mathbf{r}+\mathbf{R}) = \eta_i(\mathbf{r})e^{4i\chi_0(\mathbf{r},\mathbf{R})}. \quad (j=+,-,z). \quad (10)$$

Starting from initial states in Eq. (9), we solve Eqs. (1) and (5) alternately, and we obtain self-consistent solutions of the MH vortex lattice for η_+, η_-, and η_z under a given unit cell of the vortex lattice.[20,21] The unit cell is divided to 82×82 mesh points, where we obtain the quasiclassical Green's functions and $\Delta(\mathbf{r},\mathbf{k})$. When we solve Eq. (1) by the Riccati method,[22] we estimate $\Delta(\mathbf{r})$ at arbitrary positions by the interpolation from their values at the mesh points and by the periodic boundary condition in Eq. (10). In figures of this paper, we presented the spatial structure of the MH vortex lattice within a unit cell including MH vortices A–D as shown in Fig. 1(c), where we use coordinates X and Y rotated by 45° from the original coordinates x and y.

Using the obtained self-consistent solutions, the mass current is given by

$$\mathbf{j}(\mathbf{r}) = (j_x,j_y,j_z) \propto T\sum_{0<\omega_n}\langle\hat{\mathbf{v}}\ \mathrm{Im}\ g\rangle_{\mathbf{k}}. \quad (11)$$

When we calculate the quasiparticle states, we solve Eq. (1) with $i\omega_n\to E+i\delta$. We typically use $\delta=0.01$, which is small smearing effect of energy by scatterings. The local DOS (LDOS) for quasiparticles is obtained as

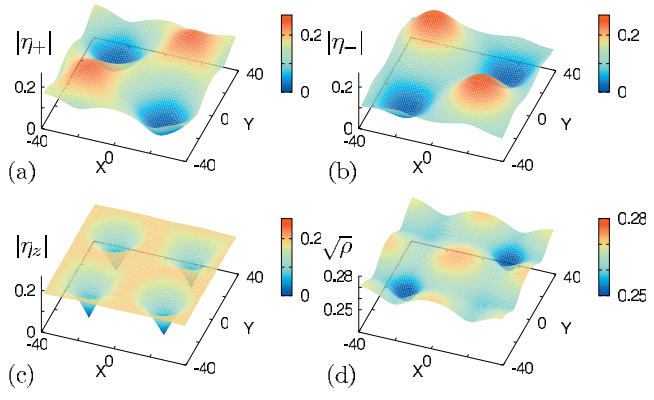

FIG. 2. (Color) Spatial structure of order parameters (a) $|\eta_+(\mathbf{r})|$, (b) $|\eta_-(\mathbf{r})|$, (c) $|\eta_z(\mathbf{r})|$, and (d) pair amplitude $\sqrt{\rho(\mathbf{r})}$ within a unit cell, obtained by self-consistent Eilenberger theory. $\Omega=0.004\Omega_0$ and $T=0.9T_c$. $\mathrm{MH}_\uparrow$ vortices A and B are located at maximum of $|\eta_+(\mathbf{r})|$, and $\mathrm{MH}_\downarrow$ vortices C and D are located at minimum of $|\eta_+(\mathbf{r})|$ in (a).

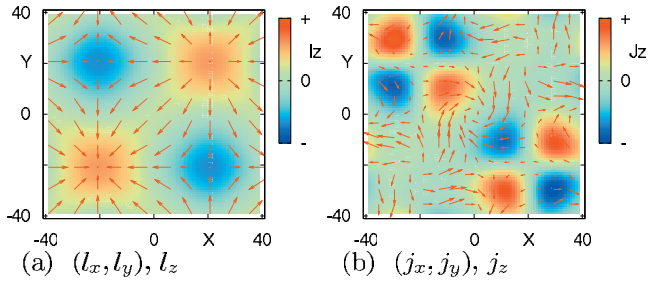

FIG. 3. (Color) Spatial structure of (a) l vector, and (b) current $\mathbf{j}$ within a unit cell, obtained by self-consistent Eilenberger theory. $\Omega=0.004\Omega_0$ and $T=0.9T_c$. Arrows indicates vectors (l_x,l_y) or (j_x,j_y), and color densities are for l_z or j_z.

$$N(\mathbf{r},E) = N_0\langle \mathrm{Re}\{g(\omega_n,\mathbf{k},\mathbf{r})|_{i\omega_n\to E+i\delta}\}\rangle_{\mathbf{k}}. \quad (12)$$

III. STRUCTURE OF ORDER PARAMETER AND MASS CURRENT

We start to discuss the structure of the pair potential. Figures 1(b) and 2 present self-consistent results for spatial structures of MH vortex lattice at $T=0.9T_c$ and $\Omega=0.004\Omega_0$, where intervortex distance is about $40R_0$. R_0 is in the order of coherence length. Around $\mathrm{MH}_\uparrow$ vortices at A and B with phase winding $(w_+,w_z,w_-)=(0,1,2)$ around each vortex center, $|\eta_z|\propto r$ and $|\eta_-|\propto r^2$ as a function of the radius r from the vortex center. Since $|\eta_+|\neq0$ at the vortex center, these vortices are coreless vortices with positive l_z [see Fig. 1(b)]. The other two $\mathrm{MH}_\downarrow$ vortices at C and D with phase winding $(w_+,w_z,w_-)=(2,1,0)$ around each vortex center are also coreless vortices but with negative l_z since $|\eta_-|\neq0$ at the vortex center.

In our calculation, as dipole length[7,8] is infinity, the vortex core radius is in the order of intervortex distance, even changing Ω. This is a character of coreless vortex. In contrast, if we calculate the vortex structure in a single component (for example, if we set $\eta_+=\eta_-=0$), the core radius of the singular vortex is small, i.e., in the order of coherence length. The pair amplitude $\rho(\mathbf{r})$ in Fig. 2(d) is almost constant but it is slightly suppressed at vortex core in the self-consistent calculations. This suppression of $\rho(\mathbf{r})$ is stronger at $\mathrm{MH}_\uparrow$ of positive l_z at A and B, compared with $\mathrm{MH}_\downarrow$ of negative l_z at C and D, which is closely related to the existence of low-lying excitations in $\mathrm{MH}_\uparrow$, not in $\mathrm{MH}_\downarrow$, as discussed later. We note that the differences of $\mathrm{MH}_\uparrow$ and $\mathrm{MH}_\downarrow$

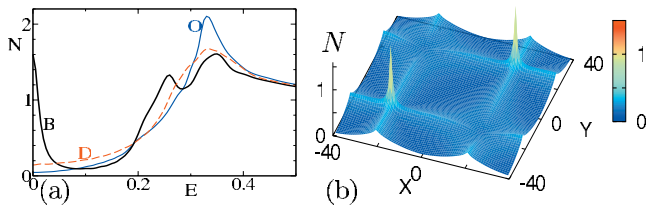

FIG. 4. (Color) (a) Local spectrum $N(\mathbf{r},E)$ of quasiparticle states at vortex center of $\mathrm{MH}_\uparrow$ (B in Fig. 1), vortex center of $\mathrm{MH}_\downarrow$ (D), and midpoint between vortices (O). (b) Zero-energy LDOS $N(\mathbf{r},E=0)$ within a unit cell. $\Omega=0.004\Omega_0$ and $T=0.9T_c$.

vortices come from the relative orientation of l vector and the angular velocity of rotation. Since the angular velocity points to z direction, the vortex windings at $MH_\uparrow$ vortex and $MH_\downarrow$ vortex are both positive, and total vortex winding around a unit cell in Fig. 1(c) is four (>0). Therefore, l vector is parallel to the angular velocity of rotation at the vortex core of $MH_\uparrow$ with $l_z>0$, and l vector is antiparallel to the angular velocity at the vortex core of $MH_\downarrow$ with $l_z<0$.

In Fig. 3(a), we present the texture of the l vector around the MH vortex. There, the direction of l vector rotates around the coreless vortex, keeping almost constant pair amplitude. Four vortices in a unit cell have different flow patters of l vector. $MH_\uparrow$ and $MH_\downarrow$ have different sense of l vector's 360° rotation. The current flow $\mathbf{j}$ is presented in Fig. 3(b). There, amplitude of circular current is larger around $MH_\uparrow$, and small around $MH_\downarrow$. In the MH vortex lattice, z component j_z appears due to the so-called bending current by $\nabla\times\mathbf{l}$.[7,8] There, j_z flows with fourfold symmetric pattern around $MH_\downarrow$ while j_z is small around $MH_\uparrow$.

IV. QUASIPARTICLE STATES

Those $MH_\uparrow$ and $MH_\downarrow$ vortices exhibit a distinctive low-lying excitation spectrum, depending on l_z direction. Figure 4(a) presents local spectrum $N(\mathbf{r},E)$ at positions B ($MH_\uparrow$), D ($MH_\downarrow$) and O in the unit cell of Fig. 1(c). Outside the vortex core (line O), we see typical DOS spectrum $N(E)\propto E^2$ for anisotropic superconductors with point nodes.[28] Even in the bulk states without rotation, there are low-energy quasiparticle states near $E=0$ due to the point node. Therefore, the low-energy states shift to zero-energy state by vortex contributions. At the vortex center of $MH_\uparrow$ (line B), remarkably we see sharp zero-energy peak even in a coreless vortex. This peak structure is similar to that seen in singular vortex[20,21] while the peak height is smaller. On the other hand, at $MH_\downarrow$ core (line D), there is no distinctive peak structure around $E=0$ in the vortex core region. These low-energy spectral differences by l_z directions are clearly seen in the zero-energy LDOS $N(\mathbf{r},E=0)$ within a unit cell, as in Fig. 4(b), where we see the distinctive peaks at A and B positions, corresponding to $MH_\uparrow$ vortex.

The difference between $MH_\uparrow$ vortex and $MH_\downarrow$ comes from the relative orientation of l vector and rotational angular velocity Ω of the rotation. Therefore, to see quantitative contribution of the rotational speed, in Fig. 5 we plot Ω dependence of $N(\mathbf{r},E=0)$ and $\rho(\mathbf{r})^{1/2}$ at $MH_\uparrow$ vortex at B, $MH_\downarrow$ vortex at D and the midpoint O. In the limit $\Omega\to 0$, we see that $N(\mathbf{r},E=0)\to 0$ and $\rho(\mathbf{r})$ is uniform everywhere because of coreless vortices. With increasing Ω, from $\Omega\sim 0.001\Omega_0$ we find the difference between $MH_\uparrow$ vortex at B and $MH_\downarrow$ vortex at D, coming from the relative l_z direction to the rotational angular velocity. When zero-energy states appears at the vortex core, the pair amplitude $\rho(\mathbf{r})$ is suppressed at the core. The differences of vortices of B and D become eminent toward the upper critical angular velocity Ω_{c2} ($\sim 0.3\Omega_0$ at $T=0.9T_c$).

As shown by line B in Fig. 5(b), around $MH_\uparrow$ vortices, $|\eta_+|(\sim\sqrt{\rho})$ is significantly suppressed at $\Omega\sim 0.04\Omega_0$. There two vortex-antivortex phase singularity appears in $\eta_+(\mathbf{r})$ at

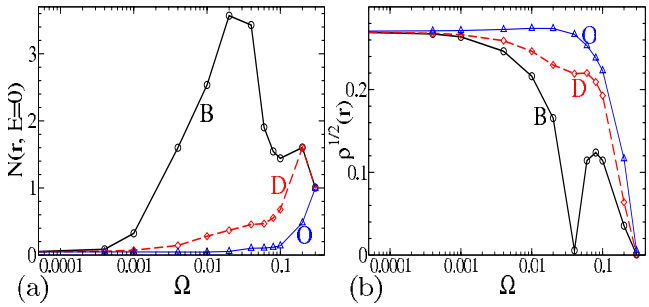

FIG. 5. (Color online) Ω dependence of (a) zero-energy LDOS $N(\mathbf{r},E=0)$ and (b) pair amplitude $\rho^{1/2}(\mathbf{r})$ at positions B (vortex center of $MH_\uparrow$), D (vortex center of $MH_\downarrow$), and O (midpoint between vortices). Horizontal axis for Ω is log scale.

the vortex core of $MH_\uparrow$. At the higher $\Omega(>0.04\Omega_0)$, the vortex-antivortex phase singularities moves to around $MH_\uparrow$ vortices, and $\sqrt{\rho}$ at vortex center B increases again. There, basal plane component (l_x,l_y) of l vector is directed to opposite direction between inside and outside around each $MH_\uparrow$ vortex at A and B.

V. BOGOLIUBOV-DE GENNES CALCULATIONS

In order to understand the fundamental difference in excitation spectrum between two MH vortices $MH_\uparrow$ and $MH_\downarrow$, we have performed the full quantum mechanical calculations based on BdG theory, assuming a single vortex in a system.[13,29] To obtain quasiparticle eigenstates labeled by (ν,k_z) and eigenenergy E_{ν,k_z}, we solve the BdG equation[30]

$$\int d\mathbf{r}_2 \begin{bmatrix} H_0(\mathbf{r}_1,\mathbf{r}_2) & \Delta(\mathbf{r}_1,\mathbf{r}_2) \\ \Delta^*(\mathbf{r}_1,\mathbf{r}_2) & -H_0(\mathbf{r}_1,\mathbf{r}_2) \end{bmatrix} \begin{bmatrix} u_{\nu,k_z}(\mathbf{r}_2) \\ v_{\nu,k_z}(\mathbf{r}_2) \end{bmatrix} = E_{\nu,k_z} \begin{bmatrix} u_{\nu,k_z}(\mathbf{r}_1) \\ v_{\nu,k_z}(\mathbf{r}_1) \end{bmatrix}, \tag{13}$$

where $H_0(\mathbf{r}_1,\mathbf{r}_2)$ is the kinetic energy term $H_0(\mathbf{r}_1,\mathbf{r}_2)=-\delta(\mathbf{r}_1-\mathbf{r}_2)\{\nabla_1^2/2m-E_F\}$ with the Fermi energy $E_F=k_F^2/2m$. The pair potential $\Delta(\mathbf{r}_1,\mathbf{r}_2)$ is expanded to the Fourier series with respect to the relative coordinate $\mathbf{r}_1-\mathbf{r}_2$ as

$$\Delta(\mathbf{r}_1,\mathbf{r}_2)=\int \frac{d\mathbf{k}}{(2\pi)^3}\Delta(\mathbf{r},\mathbf{k})e^{i\mathbf{k}\cdot(\mathbf{r}_1-\mathbf{r}_2)}, \tag{14}$$

where $\mathbf{r}=(\mathbf{r}_1+\mathbf{r}_2)/2$ is the center-of-mass coordinate. Here, we assume the coefficient $\Delta(\mathbf{r},\mathbf{k})$ to be expanded in terms of the p-wave channel as

$$\Delta(\mathbf{r},\mathbf{k})=\frac{1}{\sqrt{3}}\sum_{m=0,\pm 1}\eta_m(\mathbf{r})\varphi_m(\mathbf{k})e^{-(k^2-k_F^2)\xi_p^2} \tag{15}$$

with the factor $\varphi_m(\mathbf{k})$ defined in Eqs. (3) and (4). This is same as the expression in Eq. (2), except for the additional factor $e^{-(k^2-k_F^2)\xi_p^2}$ with the pairing size $\xi_p=k_F^{-1}$. This factor is necessary for the BdG Eq. (13) to be Hermitian.[30]

Since z dependence of the pair potential is uniform, we can set the wave function as

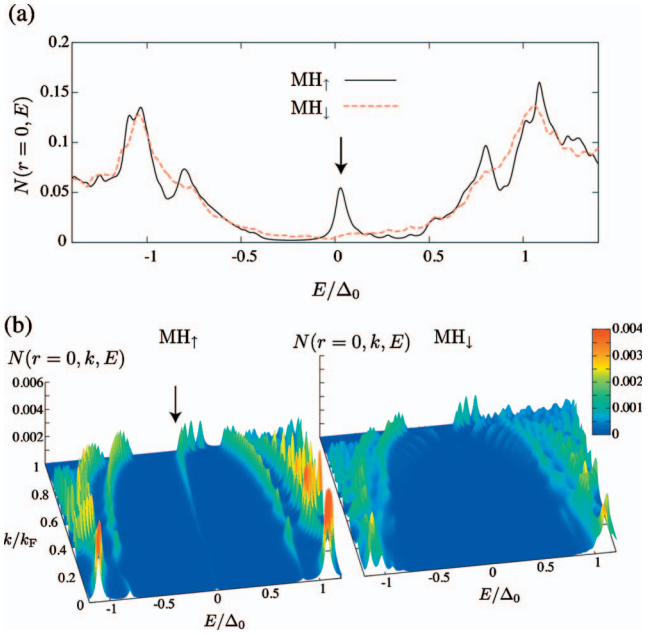

FIG. 6. (Color) LDOS $N(\mathbf{r},E)$ (a) and k_z-resolved LDOS $N(\mathbf{r},k_z,E)$ (b) at the vortex center $r=0$ of $MH_\uparrow$ and $MH_\downarrow$ in the BdG theory. $T=0$, $R=40k_F^{-1}$, and $k_F\xi=10$. $MH_\uparrow$ has a low-energy peak (assigned by arrow) inside the gap. In (b), gapedge narrows toward $k_z=k_F$ because point nodes situate at north and south poles at $k_z=\pm k_F$ on the Fermi sphere.

$$\begin{bmatrix} u_{\nu,k_z}(\mathbf{r}) \\ v_{\nu,k_z}(\mathbf{r}) \end{bmatrix} = \begin{bmatrix} \tilde{u}_{\nu,k_z}(\mathbf{r}) \\ \tilde{v}_{\nu,k_z}(\mathbf{r}) \end{bmatrix} e^{ik_z z}. \tag{16}$$

To reproduce the pair potential of MH vortex discussed in previous sections, the order-parameter profiles are given by

$$(\eta_+, \eta_0, \eta_-) = \Delta_0 e^{i\phi}(e^{\mp i\phi}(1 \pm \cos\beta),$$

$$\sqrt{2}\sin\beta,\ e^{\pm i\phi}(1 \mp \cos\beta))$$

with $\beta(r)=\pi r/2R$ for $MH_\uparrow$ and $MH_\downarrow$, respectively.[17] From wave functions and eigenenergies obtained by the BdG equation, we calculate the LDOS $N(\mathbf{r},E)$ as

$$N(\mathbf{r},E) = \sum_{k_z} N(\mathbf{r},k_z,E) = \sum_{\nu,k_z} |u_{\nu,k_z}(\mathbf{r})|^2 \delta(E - E_{\nu,k_z}). \tag{17}$$

Here, $N(\mathbf{r},k_z,E)$ is k_z-resolved LDOS and the energy is presented in a unit of the gap amplitude's constant Δ_0.

At fist sight we expect no difference between $MH_\uparrow$ and $MH_\downarrow$ because here we assume that the pair amplitude $\rho(\mathbf{r})$ is identical. The MH vortex is almost the A phase like everywhere and coreless. However, when we see the LDOS $N(\mathbf{r},E)$ by BdG theory shown in Fig. 6(a), zero-energy peak appears at the vortex core of $MH_\uparrow$, and it does not exist at $MH_\downarrow$ vortex. This quasiparticle structure is consistent to the result of Fig. 4 by Eilenberger theory. The small suppression of $\rho(\mathbf{r})$ obtained by self-consistent calculation in Sec. III is a result from the low-energy quasiparticle states $N(\mathbf{r},E)$.

To discuss the origin of zero-energy LDOS, $N(\mathbf{r},E)$ is decomposed to contributions from each k_z on the Fermi surface. The k_z-resolved LDOS $N(\mathbf{r},k_z,E)$ at the vortex core for $MH_\uparrow$ and $MH_\downarrow$ are displayed in Fig. 6(b). There, distinctive zero-energy peak only for $MH_\uparrow$ grows as $|k_z|$ increases, indicating that the low-energy excitations come from near the poles of the Fermi sphere. In contrast, there is no peak inside the gap for $MH_\downarrow$. The physical reason is due to the interplay between IAM and vortex-winding number: $(w_+,w_z,w_-)=(0,1,2)$ for $MH_\uparrow$ and (2,1,0) for $MH_\downarrow$. The IAM has the phase winding $(u_+,u_z,u_-)=(1,0,-1)$ around the Fermi surface for each pairing component $(\varphi_+,\varphi_z,\varphi_-)$.

To discuss the possibility of low-energy bound states at the vortex core, we consider effective pair potential for quasiparticles around vortex cores. The quasiparticles propagating to the angular direction around a vortex feel effective pair potential $\Delta(\mathbf{r},\mathbf{k})$ with $\phi_k \to \phi+\pi/2$. For $MH_\uparrow$, $|\Delta(\mathbf{r},\mathbf{k})_{\phi_k\to\phi+\pi/2}|^2=6|\Delta_0|(\sin^2\theta_k+\sin^2\beta\cos^2\theta_k)$ is an increasing function of r, and quasiparticles feel larger confinement potential at vortex when $|k_z|(\propto|\cos\theta_k|)$ is larger. This is the origin of zero-energy peak in the LDOS coming from near poles of the Fermi sphere. On the other hand, for $MH_\downarrow$, $|\Delta(\mathbf{r},\mathbf{k})_{\phi_k\to\phi+\pi/2}|^2 = 6|\Delta_0|\{\sin^2\theta_k - \frac{1}{2}\sin 2\phi \sin 2\beta \sin 2\theta_k + \sin^2\beta(\cos^2\theta_k - \sin^2 2\phi \sin^2\theta_k)\}$. This effective pair potential breaks circular symmetry and does not have minimum at vortex center. This implies no bound states inside the gap for $MH_\downarrow$, as shown in right side of Fig. 6(b). In essence this interplay between IAM and vortex winding yields the following algebra symbolically for the phase factors: $(w_+,w_z,w_-) + (u_+,u_z,u_-) = (0,1,2)+(1,0,-1) \to (1,1,1)+(0,0,0)$ for $MH_\uparrow$ while $(2,1,0)+(1,0,-1)\to(1,1,1)+(2,0,-2)$ for $MH_\downarrow$. The former (0,0,0) gives rise to a vortex bound state similar to the singular hard core vortex form by Caroli-de Gennes-Matricon (CdGM) (Ref. 31) while the latter (2,0,−2) yields the angle-dependent escaping form $e^{i2\phi}+e^{-i2\phi}\propto\cos 4\phi$.

As for the problem whether the zero-energy quasiparticles at $MH_\uparrow$ is Majorana state or not, the energy level of this state is slightly lifted to positive energy in the order of Δ^2/E_F in the BdG theory (E_F is Fermi energy), as shown in Fig. 6(a). This is a character of CdGM states[31,32] and also confirmed by the energy distribution of discretized eigenenergy, roughly given as $(n+\frac{1}{2})\Delta^2/E_F$ with integer n, obtained from the BdG equation. That is, this CdGM state is not Majorana state which should exist exactly at $E=0$.[13,29] This is understandable from the vortex winding of each pairing component. For the Majorana state to appear, the chiral components of $p_\pm$ should have odd winding number.[29] However, for $MH_\uparrow$, winding $(w_+,w_z,w_-)=(0,1,2)$ does not satisfy this criterion.

VI. SUMMARY AND DISCUSSIONS

In summary, we have studied the detailed spatial structure of Mermin-Ho vortex lattice state in A phase of superfluid ^{3}He, as a representative and concrete example of the skyrmion lattice. In Mermin-Ho vortex lattice, there are two types of vortices; $MH_\uparrow$ with positive l_z and $MH_\downarrow$ with negative l_z. The differences between $MH_\uparrow$ vortex and $MH_\downarrow$ vortex among the Mermin-Ho vortices come from the orientation of the local intrinsic angular momentum $\mathbf{l}=(l_x,l_y,l_z)$ at the vortex core, i.e., parallel or antiparallel to the angular velocity of rotation. Due to the orientation of l vector relative to the

rotation, Mermin-Ho vortices have different structures. By self-consistent Eilenberger theory we clarified how the intrinsic angular momentum effect of local **l** orientation appears in the structure of order parameters, current flow and quasiparticle states around coreless Mermin-Ho vortex states. These effects depending on the local l_z orientation become eminent with increasing angular velocity of rotation. The different current flows (j_x, j_y, j_z) between $MH_\uparrow$ and $MH_\downarrow$ can be used to distinguish two types of vortices in the MH vortex lattice. It is noted that zero-energy states appear at the coreless vortex of positive l_z only. These properties of quasiparticle states were also confirmed by our calculation of Bogoliubov-de Gennes theory. The differences of low-energy states between $MH_\uparrow$ and $MH_\downarrow$ are interesting also in the relation to the dissipation mechanism at the vortex core. It may be detected by magnetic resonance imaging (MRI) technique,[33] which is to probe Fermionic excitations locally. In the MRI technique, the local position of the signal can be identified by the analysis of resonance fields under the gradient of the applied magnetic field. After the position of the Mermin-Ho vortex is identified, the local low-energy quasiparticle states are measurable by the relaxation experiment of NMR at the resonance field. If the vortex has zero energy quasiparticle states, we expect rapid relaxation at the vortex core. We expect that among two types of Mermin-Ho vortices, one of them ($MH_\uparrow$) has rapid relaxation of NMR at the vortex core, and the other $MH_\downarrow$ has only slow relaxation. The present study prompts us to explore other topological objects in condensed-matter systems, such as MnSi and $Fe_{1-x}Co_xSi$ where a similar skyrmion lattice is realized.[5,6] Their electronic structure may be quite interesting. The local structure of skyrmion can be different depending on the relative orientation of applied fields.

ACKNOWLEDGMENT

The authors are grateful for useful discussions with T. Fujita and T. Ohmi.

[1] A. M. Polyakov, *Gauge Fields and Strings* (Harwood, London, 1987).
[2] T. Senthil, A. Vishwanath, L. Balents, S. Sachdev, and M. P. A. Fisher, Science **303**, 1490 (2004).
[3] U. Al Khawaja and H. Stoof, Nature (London) **411**, 918 (2001).
[4] T. Mizushima, K. Machida, and T. Kita, Phys. Rev. Lett. **89**, 030401 (2002).
[5] S. Mühlbauer, B. Binz, F. Jonietz, C. Pfleiderer, A. Rosch, A. Neubauer, R. Georgii, and P. Böni, Science **323**, 915 (2009).
[6] X. Z. Yu, Y. Onose, N. Kanazawa, J. H. Park, J. H. Han, Y. Matsui, N. Nagaosa, and Y. Tokura, Nature (London) **465**, 901 (2010).
[7] M. M. Salomaa and G. E. Volovik, Rev. Mod. Phys. **59**, 533 (1987).
[8] D. Vollhardt and P. Wölfle, *The Superfluid Phase of Helium 3* (Taylor & Francis, London, 1990).
[9] N. Read and D. Green, Phys. Rev. B **61**, 10267 (2000).
[10] S. B. Chung and S. C. Zhang, Phys. Rev. Lett. **103**, 235301 (2009).
[11] Y. Nagato, S. Higashitani, and K. Nagai, J. Phys. Soc. Jpn. **78**, 123603 (2009).
[12] G. E. Volovik, JETP Lett. **90**, 587 (2009).
[13] T. Mizushima, M. Ichioka, and K. Machida, Phys. Rev. Lett. **101**, 150409 (2008), and references therein.
[14] N. D. Mermin and Tin-Lun Ho, Phys. Rev. Lett. **36**, 594 (1976).
[15] Ü. Parts, J. M. Karimäki, J. H. Koivuniemi, M. Krusius, V. M. H. Ruutu, E. V. Thuneberg, and G. E. Volovik, Phys. Rev. Lett. **75**, 3320 (1995).
[16] R. Ishiguro, O. Ishikawa, M. Yamashita, Y. Sasaki, K. Fukuda, M. Kubota, H. Ishimoto, R. E. Packard, T. Takagi, T. Ohmi, and T. Mizusaki, Phys. Rev. Lett. **93**, 125301 (2004).
[17] T. Fujita, M. Nakahara, T. Ohmi, and T. Tsuneto, Prog. Theor. Phys. **60**, 671 (1978).
[18] J. M. Karimäki and E. V. Thuneberg, Phys. Rev. B **60**, 15290 (1999).
[19] G. Eilenberger, Z. Phys. **214**, 195 (1968).
[20] M. Ichioka, N. Hayashi, and K. Machida, Phys. Rev. B **55**, 6565 (1997).
[21] M. Ichioka and K. Machida, Phys. Rev. B **65**, 224517 (2002).
[22] P. Miranović, M. Ichioka, and K. Machida, Phys. Rev. B **70**, 104510 (2004).
[23] T. Mizushima, N. Kobayashi, and K. Machida, Phys. Rev. A **70**, 043613 (2004).
[24] N. Schopohl, J. Low Temp. Phys. **41**, 409 (1980).
[25] J. W. Serene and D. Rainer, Phys. Rep. **101**, 221 (1983).
[26] M. Fogelström and J. Kurkijärvi, J. Low Temp. Phys. **98**, 195 (1995).
[27] J. A. Sauls and M. Eschrig, New J. Phys. **11**, 075008 (2009).
[28] M. Sigrist and K. Ueda, Rev. Mod. Phys. **63**, 239 (1991).
[29] T. Mizushima and K. Machida, Phys. Rev. A **81**, 053605 (2010).
[30] T. Mizushima and K. Machida, Phys. Rev. A **82**, 023624 (2010).
[31] C. Caroli, P. G. de Gennes, and J. Matricon, Phys. Lett. **9**, 307 (1964).
[32] N. Hayashi, T. Isoshima, M. Ichioka, and K. Machida, Phys. Rev. Lett. **80**, 2921 (1998).
[33] K. Sinokita, R. Toda, and Y. Sasaki, J. Phys.: Conf. Ser. **150**, 012041 (2009).